Dynamic relaxation process of a 3D super crystal structure in a Cu:KTN crystal

Quanxin Yang (杨全鑫)[1], Xin Zhang (张欣)[2], Hongliang Liu (刘洪亮)[1,*], Xuping Wang (王旭平)[3], Yingying Ren (任莹莹)[4], Shan He (何珊)[1], Xiaojin Li (李小金)[1], and Pengfei Wu (武鹏飞)[1,]**

[1]*Tianjin Key Laboratory of Optoelectronic Sensor and Sensing Network Technology, Institute of Modern Optics, Nankai University, Tianjin 300071, China*

[2]*Hubei Key Laboratory of Low Dimensional Optoelectronic Materials and Devices, Hubei University of Arts and Science, Xiangyang 441053, China*

[3]*Advanced Materials Institute, Qilu University of Technology (Shandong Academy of Sciences), Jinan 250014, China*

[4]*Shandong Provincial Engineering and Technical Center of Light Manipulations & Shandong Provincial Key Laboratory of Optics and Photonic Device, School of Physics and Electronics, Shandong Normal University, Jinan 250358, China*

**Corresponding author: drliuhl@nankai.edu.cn; **corresponding author: pwu@nankai.edu.cn*

Received September 3, 2019; accepted November 1, 2019; posted online January 6, 2020

In this Letter, we report the existence and relaxation properties of a critical phenomenon on called a 3D super crystal that emerges at $T = T_C - 3.5°C$, that is, in the proximity of the Curie temperature of a Cu:KTN sample. The dynamics processes of a 3D super crystal manifest in its formation containing polarized nanometric regions and/or polarized clusters. However, with strong coupling and interaction of microcomponents, the characteristic relaxation time measured by dynamic light scattering demonstrates a fully new relaxation mechanism with a much longer relaxation time. As the relaxation mechanism of a relaxator is so-far undetermined, this research provides a novel perspective. These results can help structure a fundamental theory of ferroelectric relaxation.

Keywords: KTN; relaxation time; dynamic light scattering; micronano structure.

doi: 10.3788/COL202018.021901.

In the past half century, potassium tantalate-niobate (KTN) crystals have attracted a lot of attention in the research and application field because of their exceptional electro-optic (EO) properties and wide transparent wavelength range[1–8]. Thus, they have been used in EO modulation[2,5], beam deflection[6–8], electric-controlled lenses[9], and so on. Recent research shows that in the proximity of the Curie temperature, a KTN crystal presents enhanced EO properties and a few kinds of fascinating critical phenomena, i.e., giant EO effects[7,10], scale-free optics and anti-diffraction beam propagation[11,12], solitons[13,14], extreme nonlinearity[15], and 3D super crystals[13,16–19]. The origin of the distinctive phenomena of a KTN crystal is attributed to polarized nanometric regions (PNRs)[20]. PNRs emerge as the paraelectric-ferroelectric phase transition takes place in relaxation ferroelectric materials, and are deemed a characteristic of a relaxator. PNRs are similar to macroscopic ferroelectric domains, but with much smaller regions. That makes PNRs possess polarization and dynamics, and thereby provides a physical basis for the mentioned novel phenomena[21].

Among all the mentioned phenomena, the 3D super crystal has become a hotspot. That phenomenon appears in a KTN sample with a built-in one-dimensional (1D) compositional oscillating seed[22,23]. In this kind of KTN, as the paraelectric-ferroelectric phase transition takes place, simultaneously that built-in 1D order is transferred to the whole volume with the same spatial scale. The formed 3D structure can cause an optical diffraction phenomenon similar to typical X-ray diffraction since the scale of this structure and the wavelength of visible light are numerically close, just as the relationship of a crystal lattice and X-ray[24].

Theory of paraelectric-ferroelectric relaxation phase transition is not certainly defined[19], and an important method to clarify it is to measure the relaxation time of PNRs/polarized clusters. With the measured relaxation time, the relaxation process can be described by a sum of relaxation functions. A 3D super crystal is essentially dynamic relaxation, which can be illustrated by some kinds of relaxation functions with a main characteristic relaxation time[19,25–27]. The technique used in this experiment is dynamic light scattering (DLS), a technique that has been applied in the field of particle diameter measurement or size distribution profile in a suspension or polymers in a solution[28–31], also known as photon correlation spectroscopy (PCS) or quasi-elastic light scattering (QELS).

The Cu-doped KTN, $KTa_xNb_{1-x}O_3$:Cu ($x = 0.372$, $T_C = 15°C$) sample used in this experiment is grown by the off-center top-seeded solution-growth (TSSG) method with a 1D grating period of 1.52 μm along the y direction. 0.1% (mole fraction) Cu ions are doped onto the crystal to improve the dielectric property by decreasing the resistance of the grains[32]. The as-grown crystal is cut into a cuboid shape with 3.38 mm (x) × 1.89 mm (y) × 5.73 mm (z) along the basic crystallographic directions, with each face optically polished. The Curie temperature is determined at the peak of the relative permittivity curve

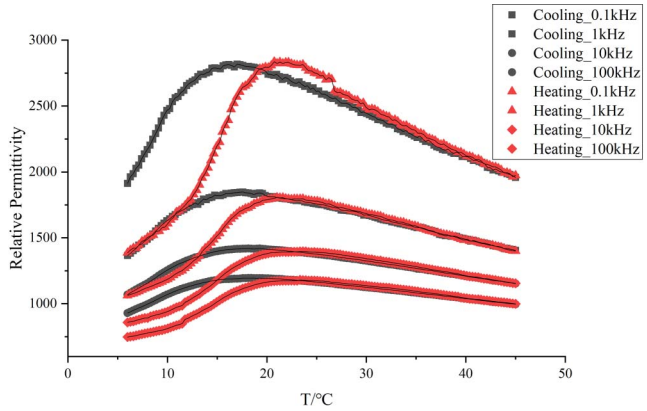

Fig. 1. Variation of relative permittivity against temperature and measurement frequency. Measurement is accomplished by a Tonghui 2830 LCR (inductance, capacitance, resistance) meter with $1V_{pp}$ sinusoidal signals at different frequencies. Thermal hysteresis loops are shown because of the crystal's relaxor ferroelectric. As shown, data at decreasing temperatures are smoother, and as frequency increases, the whole intensity decreases without a change of curve shapes.

as the temperature changes, which is 15°C in our experiment, as shown in Fig. 1.

The whole process works in the following way[29,30]. Initially, a laser beam goes through a polarizer and enters the crystal sample, and then suffers a diffraction effect caused by the 3D super crystal[26]. Then diffraction light with a specific diffraction angle travels through the second polarizer (which has a vertical polarization angle with respect to the first one) and then is collected by a photomultiplier tube (PMT). The signal is transferred to a computer for further processing and analysis, as shown in Fig. 2.

As microstructures of the 3D super crystal in the sample are undergoing relaxation dynamics[16,17], the intensity of scattering light gained by the PMT will fluctuate.

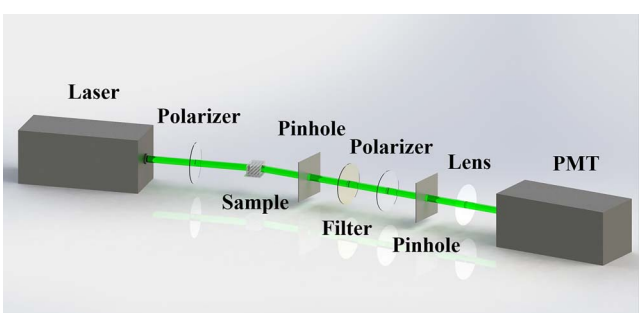

Fig. 2. Sketch of the DLS experiment setup. A light beam with a 532 nm wavelength generated by a laser is first polarized and then shot into the crystal sample. After suffering strong diffraction in the sample, the light beam changes its direction. The pinholes and filter behind the sample make sure a light beam with a special direction can get through. Two polarizers with a V-H (vertical and horizontal) setup can pick up the light signal that has been influenced by the super crystal structure. To increase the capturing efficiency of the light signal, a lens is localized in front of the PMT.

So, in the time domain, information about the time scale of the structure evolution can be obtained in the fluctuating signal that the PMT outputs.

The second-order autocorrelation function can be generated from the scattering light intensity as[30]

$$G^{(2)}(\tau) = < I(t) \cdot I(t+\tau) >, \tag{1}$$

where $G^{(2)}(\tau)$ is the autocorrelation function mentioned above, $I(t)$ is the time-varying light intensity signal, and $I(t+\tau)$ is the former signal with a delay time τ. The angular brackets $<>$ represent the expected value operation.

A laser beam at 532 nm (consistent with the response interval of the PMT) is generated by a Coherent Verdi G-Series laser. The temperature of the sample is controlled by a semiconductor chilling plate with Arroyo Instruments 5305 TEC Source, which has an accuracy of 0.01°C. A Thorlabs PMT1001/M with a lossless response frequency up to 80 MHz collects light intensity data and outputs pulse signals to a Keysight DSOX6004A oscilloscope for staging.

The whole system is separated from the external environment by optical barriers. Relaxation time data corresponding to the formation process of the super crystal begin to be recorded once the temperature reaches 11.5°C. For the disruption process of the super crystal, the data begin to be recorded once the external field is applied. For characteristic relaxation time measurement, the data collection begins 10 min after the temperature reaches 11.5°C to avoid influences from the generation process. After each measurement, the sample has been heated to 50°C and kept for 15 min to eliminate the polarization history and fatigue, and then cooled to 11.5°C for the next measurement. The change rates for heating and cooling are both 3°C/min.

An important procedure of data analysis is to fit the autocorrelation function (ACF). As we all know, Debye relaxation describes the dielectric relaxation response of ideal dipoles[21]. Here we introduce the Kohlrausch–Williams–Watts (KWW) function (a variant of the Debye relaxation function) to further delineate the relaxation process[33,34]. In the time domain, the formula is

$$\phi(t) = \exp[-(t/\tau_{\mathrm{KWW}})^{\beta}] = \int_0^{\infty} \exp(-t/\tau)\rho(\tau)\mathrm{d}\tau, \tag{2}$$

where $\rho(\tau)$ represents the distribution of the relaxation time τ. The left side of the function is also called the stretched exponential function; the right side of the function means that the KWW function describes a sum of the relaxation with different characteristic time.

The PMT outputs ~10 ns pulses and the time-resolved counts of pulses represent the average light intensity in each little time zone. Though we have got the light intensity variation with time, it is so tiny compared with the full intensity of the signal that the ACF has to be applied to gain it. Actually, the ACF calculated directly is relatively

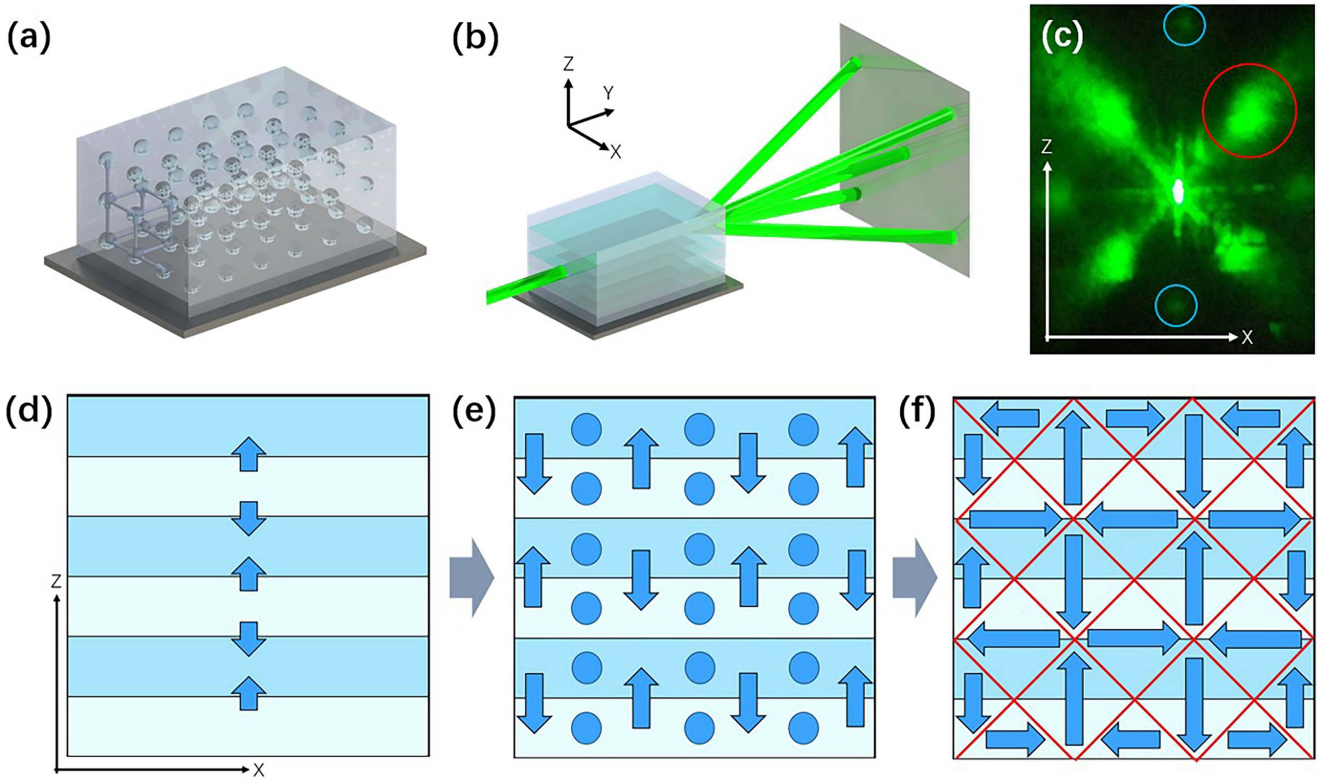

Fig. 3. (a)–(c) Diagram of the 3D dynamic super crystal and the X-ray-diffraction-like phenomenon. (a) A diagram of a dynamic 3D super crystal structure full-filling the whole column. Due to 1.52 μm period that is very similar to the wavelength of the incident light beam (532 nm), the diffraction pattern is convenient to observe and analyze. (b) Strong diffraction caused by the dynamic structure. The built-in 1D order (periodical refractive index variety) is also shown. (c) Picture of diffraction pattern captured behind the sample. Spots pointed out by blue circles correspond to the 1st-order Bragg diffraction caused by the intrinsic 1D grating, and the spot pointed out by red circle corresponds to the diffraction phenomena caused by domain walls. The latter is utilized in the DLS experiment. (d)–(f) Microscopic mechanism during dynamic structure formation. (d) PNRs with orientation vertical to the interface of different layers form. (e) PNRs with orientation vertical to the interface have strong spontaneous polarization, and those with orientation horizontal to the interface have little during dynamic relaxation process. (f) The final dynamic structure. Red lines represent 90° domain walls.

rough, and we do a re-average operation on it to acquire clear consequence. The whole calculation task is accomplished by MATLAB scripts. Raw data with scripts are available for proper purpose.

As introduced in method descriptions, there exists an intrinsic 1D grating, also called component concentration modulation along the z direction inside the as-grown crystal[16,18]. Kept at 50°C, the sample is highly transparent for its cubic phase, and its spontaneous polarization and polarization history are basically eliminated[35]. Now most incident laser beams directly propagate through the sample with the native vector direction, while a few are diffracted by the intrinsic 1D grating structure and form $\pm 1^{\text{st}}$-order Bragg diffraction patterns, as shown in the blue circles of Fig. 3(c). However, once the temperature is decreased to 11.5°C, we can observe the spontaneous formation process of a 3D super crystal structure with a consistent period of the intuition built-in 1D grating in all three dimensions, as shown in Fig. 3(a). At that time, incident laser beam suffers a strong diffraction. As a result, an X-ray diffraction-like pattern emerges in the Fraunhofer far field, as shown in Figs. 3(b) and 3(c), indicating the presence of a 3D super crystal structure. An external field can influence the stability of this dynamic structure by forcing the orientation of polarized clusters to rotate to the field direction and inducing neighboring clusters to agglomerate, forming new clusters larger in size.

The microcosmic mechanism of the 3D super crystal formation process is described here. When the sample first reaches 11.5°C ($T = T_C - 3.5$°C), as PNRs growing and combining (may form polarized clusters that are larger in size compared with PNRs), the PNRs become embedded in the layers of the sample with the same component ratio. Different phase states between different layers provide accumulated electric charge at the interface, leading to PNRs with orientation vertical to the interface form, as shown in Fig. 3(d). With an accumulated electric charge and stress at the interface and interaction between PNRs (Coulomb force), the initial structure is unstable. After relaxation for a period of time, the free energy of the whole system tends to minimize in a standard perovskite structure that represents a 90° or 180° ferroelectric domain structure. During the relaxation process, there forms microstructures with an induced dipole moment

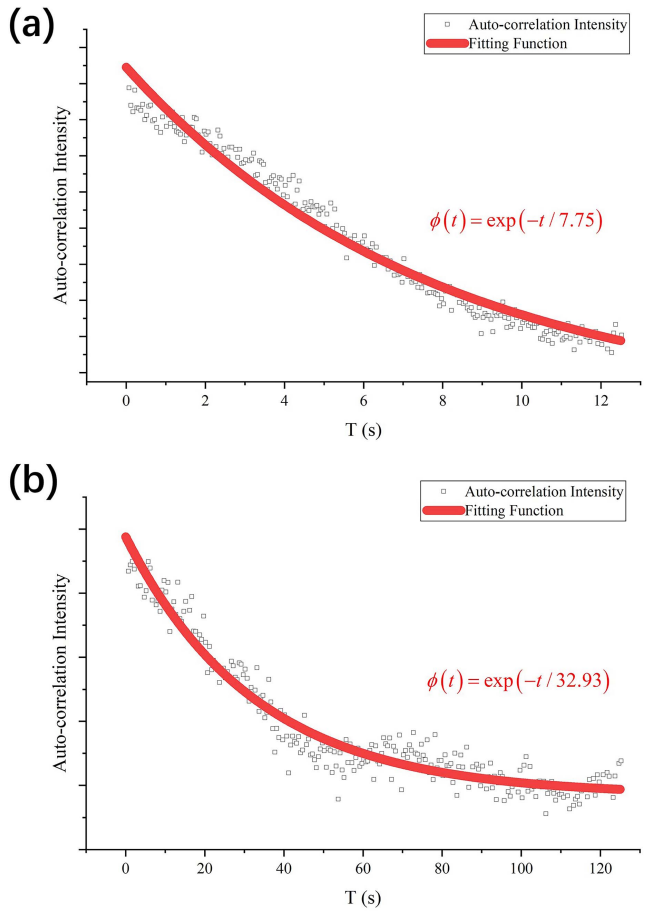

Fig. 4. Characteristic relaxation time calculated by fitting the ACF of two kinds of experiment data, equals 7.75 s and 32.93 s, respectively.

in each single layer, as shown in Fig. 3(e). Finally, the dynamic 3D structure forms, and the domain walls reveal a 90° configuration leading to the 45° 1st-order Bragg diffraction, as shown in Fig. 3(f).

The characteristic relaxation time of this kind of super crystal with respect to the KWW function is 7.75 s and 32.93 s, which means there are two kinds of relaxation models with different orders of magnitude of time. Here, the stretching parameter of the KWW function used in the fitting process is $\beta = 1$ because the graph of the ACF corresponding to that kind of relaxation phenomenon has a shape of a simple single exponential function, as shown in Fig. 4.

Characteristic relaxation time data measurement begins after the scattering light intensity is stable. Two kinds of relaxation time with different orders of magnitude of time are obtained with different data collection times: relaxation time of 7.75 s is with a data collection time of 1 min; that of 32.93 s is with a data collection time of 10 min and above. There is no valid result for shorter data collection times. We also make some measurement during the super crystal formation and disruption process. Gained relaxation times are calculated to be 49.59 s and 22.05 s for the formation and disruption process, respectively. These results share a same order of magnitude of time with the characteristic relaxation time.

As we can see, the obtained relaxation time corresponding to the intrinsic relaxation process of a 3D super crystal is longer than that of polarization clusters and PNRs, though the 3D super crystal structure is essentially formed by them. The order of magnitude of the time difference between the 3D super crystal dynamics and the original relaxation ferroelectric dynamics results from the strong coupling and interaction of the polarization clusters and PNRs. At the proper critical temperature ($T = T_C - 3.5°C$), the crystal sample forms a glassy mosaic phase with embedded polarization clusters and PNRs[16]. The dynamic order structures in a glassy disorder background restrict the response speed and frequency, making the relaxation process of the whole system become rather tardy.

Since relaxation ferroelectric materials have many incredible properties compared with general ferroelectric materials, the relaxation mechanism has become a foundational physical theory. However, though many researchers have spent lots of efforts, a perfect theorem is still absent. Our work shows that with strong coupling, interaction of microcomponents, and stickiness of a critical glassy mosaic phase disorder background, a 3D super crystal exhibits a much longer relaxation time feature compared with the inside microcomponents. Therefore, a 3D super crystal as a novel spontaneous phenomenon not only is foreseeable to be used in functional diffraction devices but also gives us a brand-new vision of the ferroelectric relaxation mechanism.

The work was supported by the National Natural Science Foundation of China (Nos. 61575097, 11704201, and 51672164), the Natural Science Foundation of Tianjin (No. 17JCQNJC01600), the Fundamental Research Funds for the Central Universities, the Open Fund of Key Laboratory of Optical Information Science & Technology (Nankai University), the Natural Science Foundation of Shandong Province (Nos. 2016ZRC01087 and ZR2017MEM016), the Achievements Transformation Project and Hubei Superior and Distinctive Discipline Group of "Mechatronics and Automobiles" (No. XKQ2018001), and the Doctoral Research Foundation Project of Hubei University of Art and Science (No. 2059039).

References

1. A. Reisman, S. Triebwasser, and F. Holtzberg, J. Am. Chem. Soc. **77**, 4228 (1955).
2. F. Chen, J. Geusic, S. Kurtz, J. Skinner, and S. Wemple, J. Appl. Phys. **37**, 388 (1966).
3. A. J. Fox, Appl. Opt. **14**, 343 (1975).
4. R. Hofmeister, A. Yariv, S. Yagi, and A. Agranat, Phys. Rev. Lett. **69**, 1459 (1992).
5. L. Zhang, V. Laur, A. Pothier, Q. Simon, P. Laurent, N. Martin, M. Guilloux-Viry, and G. Tanné, Microwave Opt. Technol. Lett. **52**, 1148 (2010).

6. T. Imai, M. Ueno, Y. Sasaki, and T. Sakamoto, Appl. Opt. **56**, 7277 (2017).
7. K. Nakamura, J. Miyazu, Y. Sasaki, T. Imai, M. Sasaura, and K. Fujiura, J. Appl. Phys. **104**, 013105 (2008).
8. J. Chao, W. Zhu, C. Wang, J. Yao, S. Yin, and R. Hoffman, Proc. SPIE **9586**, 95860T (2015).
9. T. Inagaki, T. Imai, J. Miyazu, and J. Kobayashi, Opt. Lett. **38**, 2673 (2013).
10. Y. Chang, C. Wang, S. Yin, R. Hoffman, and A. Mott, Opt. Lett. **38** 4574 (2013).
11. E. Delre, E. Spinozzi, A. J. Agranat, and C. Conti, Nat. Photon. **5**, 39 (2011).
12. E. DelRe, F. Di Mei, J. Parravicini, G. Parravicini, A. J. Agranat, and C. Conti, Nat. Photon. **9**, 228 (2015).
13. D. Pierangeli, M. Flammini, F. Di Mei, J. Parravicini, C. E. de Oliveira, A. J. Agranat, and E. DelRe, Phys. Rev. Lett. **114**, 203901 (2015).
14. D. Pierangeli, A. Tavani, F. Di Mei, A. J. Agranat, C. Conti, and E. DelRe, Nat. Commun. **8**, 1501 (2017).
15. F. Di Mei, P. Caramazza, D. Pierangeli, G. Di Domenico, H. Ilan, A. J. Agranat, P. Di Porto, and E. DelRe, Phys. Rev. Lett. **116**, 153902 (2016).
16. D. Pierangeli, M. Ferraro, F. Di Mei, G. Di Domenico, C. E. de Oliveira, A. J. Agranat, and E. DelRe, Nat. Commun. **7**, 10674 (2016).
17. F. Di Mei, L. Falsi, M. Flammini, D. Pierangeli, P. Di Porto, A. J. Agranat, and E. DelRe, Nat. Photon. **12**, 734 (2018).
18. X. Zhang, S. He, Z. Zhao, P. Wu, X. Wang, and H. Liu, Sci. Rep. **8**, 2892 (2018).
19. S. Niu, G. Joe, H. Zhao, Y. Zhou, T. Orvis, H. Huyan, J. Salman, K. Mahalingam, B. Urwin, J. Wu, Y. Liu, T. Tiwald, S. Cronin, B. Howe, M. Mecklenburg, R. Haiges, D. Singh, H. Wang, M. Kats, and J. Ravichandran, Nat. Photon. **12**, 392 (2018).
20. H. Tian, B. Yao, C. Hu, X. Meng, and Z. Zhou, Appl. Phys. Express **7**, 062601 (2014).
21. A. Bokov and Z. Ye, J. Adv. Dielectr. **02**, 1241010 (2012).
22. S. Li, P. Ju, Y. Liu, X. Jiang, R. Ni, G. Zhao, and X. Lv, Chin. Opt. Lett. **14**, 041402 (2016).
23. S. Zhu, J. Qian, and Y. Wang, Chin. Opt. Lett. **15**, 060202 (2017).
24. A. Tellal, O. Ziane, and P. L. Baldeck, Chin. Opt. Lett. **17**, 082201 (2019).
25. W. Kleemann, P. Licinio, T. Woike, and R. Pankrath, Phys. Rev. Lett. **86**, 6014 (2001).
26. R. Yan, Z. Guo, R. Tai, H. Xu, X. Zhao, D. Lin, X. Li, and H. Luo, Appl. Phys. Lett. **93**, 192908 (2008).
27. M. Zhang, Z. Guo, R. Tai, H. Luo, K. Namikawa, and J. Cao, Jpn. J. Appl. Phys. **54**, 042401 (2015).
28. R. Pecora, J. Nanopart. Res. **2**, 123 (2000).
29. K. Takahashi, S. Ohuchi, K. Saito, M. Hirasawa, and H. Sakurai, Appl. Opt. **57**, 225 (2018).
30. ISO, *Particle Characterization Including Sieving: ISO/TC 24* (ISO, 2017).
31. P. Tian, H. Chen, P. Wang, X. Liu, X. Chen, G. Zhou, S. Zhang, J. Lu, P. Qiu, Z. Qian, X. Zhou, Z. Fang, L. Zheng, R. Liu, and X. Cui, Chin. Opt. Lett. **17**, 100010 (2019).
32. X. Wang, J. Wang, Y. Yu, H. Zhang, and R. Boughton, J. Cryst. Growth **293**, 398 (2006).
33. G. Williams and D. Watts, Trans. Faraday Soc. **66**, 80 (1970).
34. F. Alvarez, A. Alegra, and J. Colmenero, Phys. Rev. B **44**, 7306 (1991).
35. Y. Li, J. Li, Z. X. Zhou, R. Y. Guo, and A. Bhalla, Ceram. Int. **40**, 1225 (2014).